molecular pharmaceutics

Article

pubs.acs.org/molecularpharmaceutics

Phytosomes Loaded with Mitomycin C–Soybean Phosphatidylcholine Complex Developed for Drug Delivery

Zhenqing Hou,*[,†,‡] Yang Li,[†,‡,§] Yuancan Huang,[†] Chunxiao Zhou,[†] Jinyan Lin,[∥] Yixiao Wang,[†] Fei Cui,[†] Shuifan Zhou,[†] Mengmeng Jia,[†] Shefang Ye,[†] and Qiqing Zhang*[,†,⊥]

[†]Department of Biomaterials, Research Center of Biomedical Engineering, College of Materials, Xiamen University, Xiamen 361005, China

[∥]Department of Materials Science and Engineering, College of Materials, Xiamen University, Xiamen 361005, China

[⊥]Institute of Biomedical Engineering, Chinese Academy of Medical Science, Peking Union Medical College, The Key Laboratory of Biomaterial of Tianjin, Tianjin 00192, China

[§]Department of Chemistry, College of Chemistry & Chemical Engineering, Xiamen University, Xiamen 361005, China

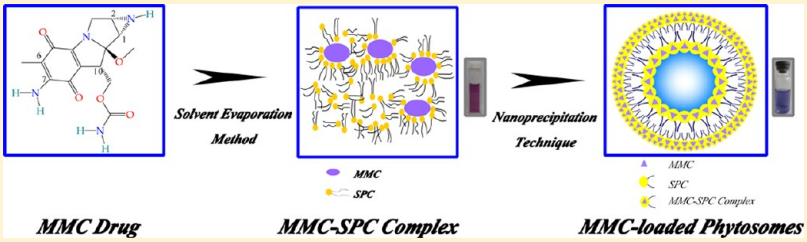

ABSTRACT: A novel formulation system of phytosomes loaded with mitomycin C–soybean phosphatidylcholine (MMC–SPC) complex (MMC-loaded phytosomes) was prepared by a solvent evaporation method combined with a nanoprecipitation technique for the purpose of development of an MMC drug delivery system. The MMC-loaded phytosomes were evaluated by average particle size, zeta-potential, and residual drug-loading content as well as an in vitro drug release profile. Furthermore, in vitro stability tests and in vitro/vivo biological evaluations of the MMC-loaded phytosomes were performed. DSC, FTIR, and XRD demonstrated that MMC interacted physically with SPC within the phytosomes. DLS and ELS described a dispersion with an average particle size of 210.87 nm, a narrow size distribution (PDI 0.251), and a zeta-potential of −33.38 mV. SEM, TEM, and AFM images showed that the MMC-loaded phytosomes were spherical and intact vesicles. In vitro stability tests demonstrated that the average particle size and residual drug-loading content of the MMC-loaded phytosomes had no evident change at different storage conditions. In vitro drug release profiles indicated biphasic behavior with an initial burst release, followed by a subsequent prolonged sustained release. In vitro cytotoxicity assays with H_{22} cells showed that the MMC-loaded phytosomes had remarkable cytotoxicity. In vivo antitumor effect of the MMC-loaded phytosomes also revealed a dose-dependent and superior curative inhibitory effect on tumor growth without loss of body weight compared to free MMC. Histopathological analysis of specimens taken from tumor tissues indicated that MMC-loaded phytosomes had lethal effect to hepatoma cell. These findings suggested that the MMC-loaded phytosomes can serve as a promising and effective formulation for drug delivery and cancer therapy.

KEYWORDS: *delivery vehicle, mitomycin C, soybean phosphatidylcholine, complex, phytosomes*

1. INTRODUCTION

Mitomycin C (MMC) is an antiproliferative and anticancer drug by virtue of its antibiotic activity, extensively used in clinical chemotherapy for the treatment of a variety of cancers including stomach, breast, pancreas, colon, and bladder cancer.[1−3] Generally, MMC is a cell cycle phase-nonspecific agent and a potent bifunctional bioreductive drug with an aziridine ring and a carbamoyl chain essential for enhanced pharmacological effects in hypoxic environments and thus great potential for local-regional treatment of tumors.[3−6] MMC is rapidly absorbed into systemic circulation. This leads to relatively low plasma levels of the drug around the effect-relevant sites with decreasing therapeutic effect and increasing toxicity risk in systemic administration, limiting great benefits against cancer therapy. A series of side effects including prolonged bone marrow suppression and severe renal damage produce a major obstacle for the introduction of MMC into wide clinical use.[3,5,7−10]

At present, drug delivery with controlled release using nanoscale delivery vehicles attracts great interest owing to the advantages of nanometer scale being beneficial for maximizing efficiency as well as minimizing side effects of the drug.[11,12] Therefore, the exploration of an effective nanosize delivery

Received: December 22, 2011
Revised: November 1, 2012
Accepted: November 16, 2012
Published: November 16, 2012

system with long-term and sustained release for MMC to overcome the toxic limitations and enhance the antitumor effect is valuable in clinical applications.

Phospholipids (PC) are a class of lipids that are a major component of all cell membranes as they can form lipid bilayers. As an amphipathic molecule, PC possessed a positively charged headgroup and two neutrally charged tail groups, a rare molecular characteristic that renders PC miscible in both water and lipid environments, in which the oxygen atom of the phosphate group has a strong tendency to gain electrons and the nitrogen atom to lose electrons.[13,14] Additionally, any kind of drug possessing an active hydrogen atom (−COOH, −OH, $-NH_2$, −NH−, ═NH, etc.) can be esterified (with or without spacer chain) to the hydroxyl group of a PC molecule, generating an amphiphilic agent to facilitate the crossing of the cell-membrane barrier.[15] Therefore, PC can be an attractive delivery vehicle, in other words, a building material of some nanoparticles for some drug molecules to enhance the absorption across lipid-rich biological barriers and increase the efficacy of drug with subsequent improved therapeutic effects. Soybean phosphatidylcholine (SPC), as an active constituent of soybean, likewise is a class of PC, generally used as a nutritional supplement to help support brain health. SPC has been clinically available for several decades, owing to these outstanding advantages including biocompatibility, biodegradability, metabolic activity, and low toxicity and cytotoxicity compared to its synthetic alternatives.[16,17] These abundant characteristics make SPC an attractive candidate for production of pharmaceutical dosage forms.

As a type of soft nanoparticle, phytosome is a lipid-compatible molecular complex. A phytosome unit is a molecular-level association, assuming a micellar shape and forming a spherical structure, overall similar to a liposome, but with a different guest localization. In a liposome unit, the active principles are water-soluble, hosted in the inner cavity, with little, if any, interaction taking place between the hydrophilic principle and the surrounding hundreds of phospholipid molecule cores. On the contrary, phytosomes involving two molecules (one phospholipid plus one drug) host their drug guest, generally little soluble both in water and in lipids, at their surface, where the polar functionalities of the lipophilic guest interact with the charged phosphate head of phospholipids via polar and hydrogen-bonding interactions.[18−20] At present, as a molecular drug delivery vehicle, the phytosome is a hybrid nanoparticle that entraps drug within SPC and resembles SPC in being substantially lipid-soluble and water-soluble, and its largely amphipathic character facilitates its transport from the surrounding water-soluble environment to the lipid-soluble environment of cancer cell membrane for increase of effectiveness. Thus the phytosome technology substantially improves the bioavailability, enhances the efficacy, and reduces the toxic side effects of drug, providing a fundamental advantage and a breakthrough for clinical application of some drugs.[14,18] With an aim to design a safe and effective phytosome, phospholipid complex has attracted more and more attention in recent years since it is the prerequisite of formation of the phytosomes. As is reported, daidzein−phospholipid complex, salvianolic acid B−phospholipid complex, clarithromycin−phospholipid complex, rutin−phospholipid complex, 10-hydroxycamptothecin−phospholipid complex, oxymatrine−phospholipid complex, luteolin−phospholipid complex, curcumin−phospholipid complex, silybin−phospholipid complex, valproic acid−phospholipid complex, and so on[14,21−31] are formed usually in a nonaqueous solvent, exhibiting outstanding advantages over pure drug in greatly enhancing the absorption into a selected tissue, markedly improving anticancer efficacy, or vastly preserving low cytotoxicities. Moreover, hydrophobic modification of hydrophilic drugs has been established as an attractive and straightforward approach to improve the liposolubility of some water-soluble drugs such as insulin, increase drug uptake through lipid-rich cell membranes, and thus enhance the therapeutic effect.[32,33] Overall, it is in general challenging, nevertheless, to prepare the well-defined molecular SPC delivery vehicles to entrap the less lipophilic drug.

The objective of this work was to formulate MMC into the phytosomes by a relatively easy-to-fabricate preparation strategy using amphiphilic nanoparticles as a cargo space to load MMC that aim at reducing its side effects, preserving its stability, and increase its antitumor effect for clinical use. We expected that these phytosomes may be a useful and injectable new drug delivery system with controlled release for MMC.

2. MATERIALS AND METHODS

2.1. Materials. All chemical reagents were of analytical grade and used without further purification unless otherwise stated. MMC (mitomycin C, purity grade = 99.5%) was purchased from Hisun Pharmaceutical Co., Ltd. (Zhengjiang, China). SPC (soybean phosphatidylcholine, purity grade >90%) was provided by Lipoid GmbH (Ludwigshafen, Germany). Dichloromethane (DCM), tetrahydrofuran (THF), and dimethyl sulfoxide (DMSO) were obtained from Sinopharm Chemical Reagent Co., Ltd. (Shanghai, China). RPMI-1640, penicillin−streptomycin, and trypsin were ordered from Sigma Chemical Corp (St. Louis, MO, USA). All solutions used in high-performance liquid chromatography (HPLC, Waters Associates, Milford, MA, USA) analysis were filtered and degassed using a 0.22 μm membrane filter with a filtration system.

2.2. Preparation and Characterization of MMC−SPC Complex. According to the literature reported by our group previously, the complex was prepared by a solvent evaporation method.[34] Briefly, 10 mg of MMC powder and 30 mg of SPC were codissolved in 12.5 mL of THF, and the resulting solution was transferred to a glass pressure vessel accompanied by vigorous agitation in a 40 °C water bath for 4 h until the formation of a clear magenta mixture was obtained. Then, THF was removed via vacuum rotary evaporation using a rotary evaporator (N-1001S-W; EYELA, Tokyo, Japan). The physical mixture of MMC and SPC was prepared at the same weight ratio by grinding them inside an agate mortar.

To evaluate the complexing rate of MMC with SPC in the formation of the MMC−SPC complex, the dryness film was dissolved in 10 mL of DCM, followed by vigorous vortexing, and filtered through a 0.22 μm Millipore membrane filter to separate free MMC precipitates and the homogeneous complex. The filtrate was evaporated, and the absolute MMC−SPC complex was determined by a HPLC system consisting of a Waters 2695 separation module and a Waters 2996 photodiode array (PDA) detector with the following conditions: stationary phase, Symmetry C18 column (250 mm × 4.6 mm, 5 μm); temperature, 25 °C; mobile phase, distilled water/methanol (65/35, v/v), freshly prepared, filtered through a 0.22 μm Millipore membrane filter before use, and degassed utilizing a sonication method; elution flow rate, 1 mL/min; detection wavelength, 365 nm. The concentration of MMC was

dx.doi.org/10.1021/mp300489p | Mol. Pharmaceutics 2013, 10, 90−101

determined on the basis of the peak area at the retention time of 7.2 min by reference to a calibration curve. The complexing rate (CR) of MMC−SPC complex was calculated by the following equation:

$$\mathrm{CR}\ (\%) = W(\mathrm{complexed})/W(\mathrm{total}) \times 100\%$$

W(complexed): the amount of the complexed MMC. W(total): the total amount of MMC added in the preparation of MMC−SPC complex.

The MMC−SPC complex was evaluated using DSC, XRD, and FTIR. Thermograms of MMC−SPC complex were evaluated to investigate the thermal behavior by DSC analysis (DSC 204F1; Netzsch, Selb, Germany) with heating cycles of the temperature range of 25−400 °C. 10 mg of MMC−SPC complex was placed in a sealed aluminum pan and heated continuously at the rate of 10 °C/min under a constant flow (10 mL/min) of nitrogen gas. MMC, SPC, and the physical mixture of MMC and SPC were compared as control.

XRD analysis of MMC−SPC complex was obtained using an X-ray diffractometer (Phillips X'pert Pro Super; Panalytical, Almelo, The Netherlands) and was evaluated to investigate the physical state of MMC in MMC−SPC complex. The X-ray diffractogram was scanned with monochromatic Cu Kα radiation generated at 30 mA tube current and 40 kV tube voltage. The scanning diffraction angle (2θ) was increasing from 5° to 60° with a step size of 0.05° and a count time of 5 s. As control, the characteristics of MMC, SPC, and the physical mixture of MMC and SPC were investigated as well. Additionally, MMC−SPC complex was dispersed in distilled water. The dispersion was frozen at −30 °C overnight and lyophilized for 24 h. The lyophilized MMC−SPC complex was investigated by XRD.

FTIR analysis (Bruker IFS-55 FTIR spectrometer; Bruker Co., Zurich, Switzerland) of MMC−SPC complex was used to investigate the interaction between MMC and SPC. The FTIR spectrum of MMC−SPC complex was determined with KBr pellets with source IR at 25 °C and obtained in the transmission mode with the wavenumber region 4000 to 750 cm^{-1} at 4 cm^{-1} spectral resolution. Besides the FTIR spectra of MMC, SPC and the physical mixture of MMC and SPC were obtained as control.

2.3. Preparation of MMC-Loaded Phytosomes. The MMC−SPC complex was formulated into the MMC-loaded phytosomes by a nanoprecipitation technique. In brief, 10 mL of DCM was added to the MMC−SPC complex (equivalent to 10 mg of MMC), followed by gentle agitation until a clear homogeneous solution used as a dispersed phase was obtained. This dispersed phase was then dropwise (0.2 mL/min) introduced into 40 mL of distilled water under moderate magnetic stirring. Subsequently, the dispersed phase gradually evaporated with stirring overnight, producing a clear suspension with light bluish opalescence, resulting in the formation of the MMC-loaded phytosomes. MMC vehicles (drug free phytosomes) were prepared in the same way except the SPC−MMC complex was replaced by SPC.

2.4. Physicochemical Characterization of MMC-Loaded Phytosomes. The average particle size and polydispersity index (PDI) of the MMC-loaded phytosomes were determined by DLS using a Malvern Zetasizer Nano-ZS (Malvern Instruments, Malvern, Worcestershire, U.K.). The zeta potential of the MMC-loaded phytosomes was obtained by ELS with Zetaplus (Malvern Instruments, Malvern, Worcestershire, U.K.). The 2D surface morphology of the MMC-loaded phytosomes was visualized by SEM (LEO 1530VP; Elektronenmikroskopie GmbH, Oberkochen, Germany) operating at an accelerating voltage of 20 kV. The morphology and structure of the MMC-loaded phytosomes were observed by TEM (JEM 2100; JEOL, Tokyo, Japan) operating at an accelerating voltage of 200 kV. The 3D surface morphology of the MMC-loaded phytosomes was visualized by AFM (Nanoscope Multimode AFM; Veeco Instruments Inc., New York, USA).

2.5. Evaluation of Lyophilized MMC-Loaded Phytosomes. The produced MMC-loaded phytosomes were added to 2% of dextran solution (w/v). The suspension was frozen at −30 °C overnight and lyophilized for 24 h using a freeze drier (Labconco Plus 12; Labconco, Kansas City, MO. USA) at a condenser temperature of −80 °C and under a vacuum of 10 Pa. The obtained lyophilized MMC-loaded phytosomes were stored in a sealed glass ampule at 4 °C for future use.

Evaluation of the lyophilized MMC-loaded phytosomes was performed by reconstituting the lyophilized products in distilled water. The average particle size, PDI, zeta potential, and residual drug-loading content (described below) of the reconstituted dispersion were determined and compared to those before lyophilization.

2.6. Residual Drug-Loading Content. The amount of drug entrapped in the MMC-loaded phytosomes was determined by HPLC analysis. Prior to analysis, 5 mg of MMC-loaded phytosomes was dissolved in 10 mL of DCM. The organic solution was filtered through a 0.22 μm Millipore membrane filter, and 20 μL of the filtrate was submitted to HPLC analysis. Therefore, the residual drug-loading content could be calculated using the following equation:

$$\text{residual drug-loading content}\ (\%) = W_N/W_0 \times 100\%$$

W_N: the amount of drug entrapped in MMC-loaded phytosomes at N days or lyophilized MMC-loaded phytosomes at N months. W_0: the amount of drug entrapped in MMC-loaded phytosomes at 0 days or lyophilized MMC-loaded phytosomes at 0 months.

2.7. In Vitro Stability Tests. A short-term stability test of the MMC-loaded phytosomes was evaluated immediately after preparation and subsequently at regular intervals. Briefly, 10 mL of MMC-loaded phytosomes was transferred into clear glass vials and stored at 25 and 4 °C, respectively for 15 days. As a vital indicator to evaluate the short-term stability of the MMC-loaded phytosomes, the residual drug-loading content was determined at predetermined time intervals (at 0, 1, 2, 3, 4, 8, and 15 days) respectively. An aqueous solution of free MMC was prepared in the same way and used for comparison.

A long-term stability test of the lyophilized MMC-loaded phytosomes was performed at 25 and 4 °C, respectively for 6 months of storage. The lyophilized MMC-loaded phytosomes were divided into 42 samples (7 samples at 25 °C per group, 3 groups in all; 7 samples at 4 °C per group, 3 groups in all), and transferred into clear glass vials in a dark place and stored for 6 months. At regular intervals (at 0, 1, 2, 3, 4, 5, and 6 months) respectively, the average particle size and residual drug-loading content were determined. Free MMC powder product was treated in the same way and used for comparison.

2.8. In Vitro Release Profiles. In vitro release of MMC from the phytosomes was analyzed by a dynamic dialysis method. The dialysis bags were used to retain the phytosomes and allow the released drug to permeate into the release medium. The experiment was conducted in a dialysis bag (M_w cutoff = 4,000 Da) with either phosphate-buffered saline (PBS)

dx.doi.org/10.1021/mp300489p | Mol. Pharmaceutics 2013, 10, 90−101

(0.02 M, pH 7.4) or 25% (v/v) mouse plasma (PBS as the solvent). The lyophilized phytosomes (equivalent to 10 mg of MMC) were dispersed in 2.5 mL of either PBS or 25% plasma, and the dispersion was added into a dialysis bag. The bag was hung inside a 120 mL Erlenmeyer flask, and then 100 mL of either 25% plasma or PBS medium was added to immerse the dialysis bag with the formulation. The system was kept on a magnetic stirrer under controlled conditions (100 rpm, 37 °C). At designated time points (0.5, 1, 2, 3, 4, 5, 6, 7, 8, and 16 h), 1 mL of the release medium was completely withdrawn and subsequently replaced with the same volume of either fresh 25% plasma or fresh PBS solution. The release medium was stored at −20 °C till analysis for the amount of released MMC by HPLC. For comparison, in vitro release of 10 mg of MMC dispersion was investigated as a control.

2.9. In Vitro Cytotoxicity Assays. The cell cytotoxicity of the MMC-loaded phytosomes against H_{22} cells was determined by an MTT assay. The cells growing in a long phase were seeded in 96-well culture plates at a density of 1×10^4 cells/well. After 24 h culture at 37 °C and 5% CO_2 atmosphere, the cells were respectively exposed to 20 μL of MMC-loaded phytosomes from low concentration (1, 3 μg/mL) to high concentrations (6, 9, and 12 μg/mL) for 24 h. Subsequently, a mixture of 20 μL of MTT solution (5 M, PBS as the solvent, pH 7.4) was added to each well. After cell incubation for an additional 4 h, supernatants were removed accompanied by the later addition of 150 μL of DMSO to each well to resuspend the cells. The assay plate was agitated on a water bath heater at 37 °C for 30 min to dissolve any formazan crystals. Absorbance at 570 nm was measured using a microplate reader (model 680; Bio-Rad Laboratories, Richmond, CA, USA). Cells treated by free MMC as a control were investigated using the same method.

2.10. In Vivo Antitumor Effects. Each of the 50 Kunming mice (clean class; 18−22 g of body weight; 4−5 weeks of age) was inoculated subcutaneously in the right axillary region with 0.2 mL of cell suspension containing 5×10^6/mL H_{22} cells before the treatment. H_{22} solid tumors were not hormone dependent and easily grown in the subcutaneous layer of male mice. The tumors were allowed to grow for 7 days after tumor transplantation, and the treatment was performed after 7 days.

The antitumor effect of the MMC-loaded phytosomes was evaluated with the tumor inhibition rate via intravenous administration in H_{22} solid tumor-bearing mice (administered 3 times at 24, 72, and 120 h after inoculation). 50 tumor-bearing mice were randomly distributed into 5 experiment groups (10 mice per group). As a negative control group, group 1 was injected with 0.2 mL of 0.9% sodium chloride injection at the same time point as in the case of all other groups. As a positive control group, group 2 was treated with a 0.2 mL injection of commercially available MMC solution at a dose of 2 mg/kg. As three experiment groups, groups 3, 4, and 5 were injected with 0.2 mL of MMC-loaded phytosomes at a series of increasing concentrations (1, 2, and 3 mg/kg, respectively), representing the low, medium, and high treatment groups. The treated mice were housed in 5 separate cages. The overall animal behaviors of every group were observed and the average body weight was examined at predetermined time intervals. After 12 days, tumor tissues were harvested and accurately weighed. The tumor inhibition rate (TIR) was calculated by the following equation:

$$\text{TIR}\ (\%) = (1 - \text{TW of tested group} / \text{TW of negative control group}) \times 100\%$$

TW: average tumor weight.

2.11. Histopathologic Analysis. 50 mice used for in vivo antitumor effect were killed for histopathologic analysis. The experimental and control fresh tumor tissues (total 5 tumor tissues) were immediately enucleated, then fixed in 10% formalin neutral buffer solution overnight, and finally rinsed with PBS. Samples were dehydrated with a graded series of increasing concentrations of ethanol (70−100%), cleared with xylene solutions, and embedded in paraffin blocks. 4 μm sections were cut with a microtome and stained with hematoxylin−eosin (HE). Representative histological images were recorded with a charge-coupled device digital camera fixed to a microscope.

2.12. Statistical Analysis. All experiments were repeated at least three times. All data were expressed as average ± SD (standard deviation) unless particularly outlined. A one-way analysis of variance (ANOVA) was performed with least-significant difference (LSD) test in statistical evaluation. The difference between two groups was considered to be significant when the p value was less than 0.05, and highly significant when the p value was less than 0.01 or 0.005.

3. RESULTS AND DISCUSSION

3.1. Preparation and Characterization of MMC−SPC Complex. The MMC−SPC complex was prepared by a solvent evaporation method. The absolute separation of free drug from the MMC−SPC complex is the prerequisite for the precise calculation of complexing rate. In our previous study,[34] the problem with MMC is that it is difficult to directly dissolve in DCM, in other words, MMC could precipitate after 24 h of storage. It is worth pointing out that the solubility of MMC within DCM could not be enhanced effectively by simple physical mixing with SPC. On the contrary, in the present study, the MMC−SPC complex is easily dissolved in DCM and stable even after 24 h of storage. The complexing rate of MMC with SPC in MMC−SPC complex was 93.66 ± 0.41%. Thus, it is hypothesized that when the hydrophobic organic solution was introduced into the MMC−SPC complex, the hydrophilic headgroup of SPC was directed toward the hydrophilic areas of MMC and the hydrophobic tail was directed toward the organic molecule to provide the correct orientation, which could facilitate its incorporation into a lipid based delivery vehicle. The explanation is further confirmed by DSC, XRD, and FTIR, which will be discussed below.

DSC is a fast tool to estimate the distribution state of drug in the pharmaceutical compound matrix. Figure 1A shows the DSC curves of MMC, SPC, the MMC−SPC physical mixture, and the MMC−SPC complex. A very sharp endothermic peak appeared at 242 °C for MMC, and a broad endothermic peak of SPC was observed at 325−375 °C. The DSC curve of the physical mixture showed an additive effect of MMC and SPC. Additionally, a relatively less intense endothermic peak of MMC can be seen clearly. On the contrary, from the DSC curve of the MMC−SPC complex, the original characteristic endothermic peak of MMC disappeared whereas a single peak different from the peaks of the individual components of the complex was observed, at the same time, the curve principally revealed a more obvious effect of SPC and a greater typical peak of SPC shifted little to a higher temperature. On the basis

dx.doi.org/10.1021/mp300489p | Mol. Pharmaceutics 2013, 10, 90−101

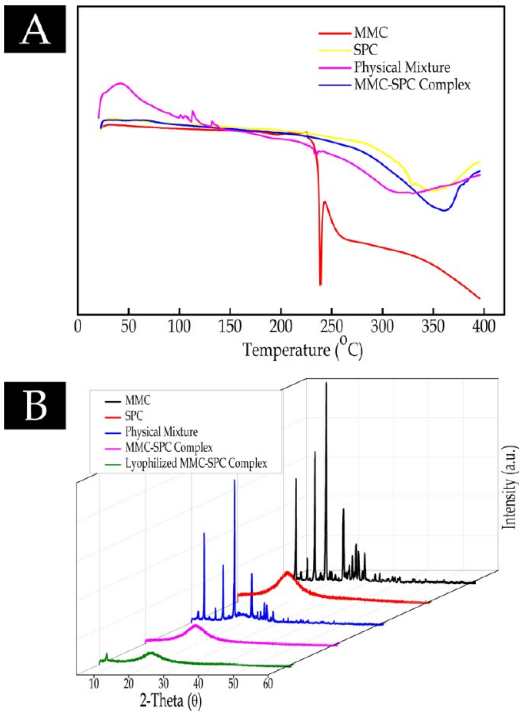

Figure 1. DSC thermograms (A) and XRD patterns (B) of MMC, SPC, MMC and SPC physical mixture, and MMC−SPC complex.

of experiments,[35,36] it can be concluded from this phenomenon that MMC may interact with SPC and the interactions should have some weak intermolecular interactions, van der Waals forces, or hydrogen bonding, singly or in combination. There is also some contribution of hydrophobic interaction attributed to the aromatic ring of MMC in the MMC−SPC interaction. Actually, the interaction of MMC with the polar headgroup of SPC molecules leads two long fatty acid chain tails of SPC to turn freely and enwrap the polar head of SPC containing the MMC molecule, thus MMC could be molecularly dispersed in SPC. The explanation remains to be proved and will be discussed below.

XRD is used to evaluate the physical state of MMC in the MMC−SPC complex. Figure 1B shows the XRD diffractograms of MMC, SPC, the physical mixture of MMC and SPC, and the MMC−SPC complex. The XRD diffractogram of MMC shows partial sharp crystalline peaks, representative of the characteristics of a molecular compound with some crystallinity, whereas a broad peak was observed in that of SPC, indicating SPC was amorphous lacking crystalline peaks. The XRD diffractogram of the physical mixture depicted that the intensity of the diffraction peaks partially decreased, however, some characteristic crystalline drug signals were still detectable, indicating that MMC as a crystalline form was retained in their physical mixture. Conversely, the characteristic crystalline peaks disappeared in the diffractogram of the complex whereas the amorphous characteristics resembled those of SPC, indicating the conversion of the crystalline form of MMC into the amorphous form, suggesting that MMC existing in the SPC matrix was either molecularly dispersed or in the amorphous form. Thus, it could be concluded that the possible interactions would have occurred between MMC and SPC in the complex. Moreover, the diffractogram of the lyophilized complex was similar to that of the complex before lyophilization, indicating that the physical state of MMC did not change in the MMC−SPC complex after lyophilization. These results combined with the previous results of DSC proved once again that, after the complexation, the oriented combination of MMC with the polar ends of SPC substantially resulted in the formation of the phospholipid complex rather than just a simple physical mixture, which is preferable for an MMC controlled release system.

The formation of the complex can be confirmed by FTIR spectroscopy comparing the spectrum of the complex with the individual components and their physical mixture. The FTIR spectra of SPC, MMC, their physical mixture, and the complex are shown in Figure 2. There was a significant difference

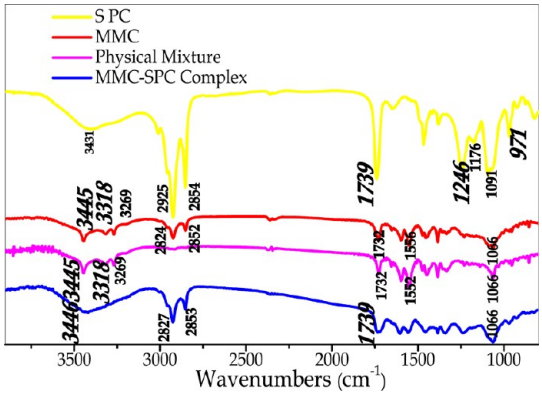

Figure 2. FTIR spectra of SPC, MMC, MMC−SPC physical mixture, and MMC−SPC complex.

between the physical mixture and the complex. The spectrum of the physical mixture also showed an additive effect of MMC and SPC. The presence of MMC in their physical mixture was revealed by two absorption peaks at 3,445 and 3,318 cm^{-1}, ascribed to the presence of $-NH_2$ and −NH− structure groups, whereas amino N−H stretching vibrations in the spectrum of MMC merged with a broad absorption peak at 3,446 cm^{-1} in that of the complex, indicating that these characteristic absorption peaks of MMC were almost shielded by that of SPC. On the other hand, the aliphatic phosphate P═O stretching vibration, evident at 1,246 cm^{-1} with a strong absorption peak in the spectrum of SPC, indicated the presence of oxygen-containing functional groups, whereas it almost disappeared in that of the complex. It could be explained that $-NH_2$ and −NH− structure groups of MMC may interact with the P═O structure group of SPC with new hydrogen bonds in the formation of the MMC−SPC complex. The absorption peak of choline quaternary ammonium $CN^{\pm}-(CH_3)_3$ groups at 971 cm^{-1} in the spectrum of SPC was shifted to high frequency in that of the MMC−SPC complex with a decreased intensity. This proved that the interaction between SPC and MMC is also at the level of the choline moiety. The absorption peak of the two long aliphatic chains of fatty acids in the SPC molecule, carbonyl C═O stretching vibration at 1,739 cm^{-1}, was not related to any change in the spectrum of the MMC−SPC complex, suggesting that the long chain fatty acids are not participating in formation of the complex. Moreover, no new significant peaks were observed in the complex. Consistent with the results of DSC and XRD analysis, these results suggested that hydrogen-bonding and other weak physical interactions between MMC and SPC play a leading role during the formation of the complex rather than just a simple physical mixture because of no appearances of new functional groups.

dx.doi.org/10.1021/mp300489p | Mol. Pharmaceutics 2013, 10, 90−101

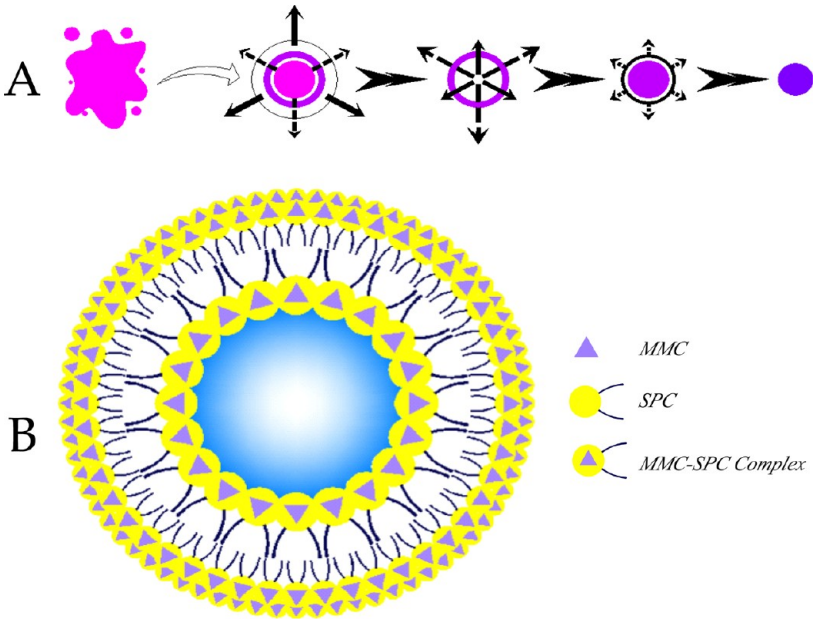

Figure 3. (A) Mechanism of a formulation of MMC-loaded phytosomes by a nanoprecipitation technique. (B) Schematic structure of MMC-loaded phytosomes.

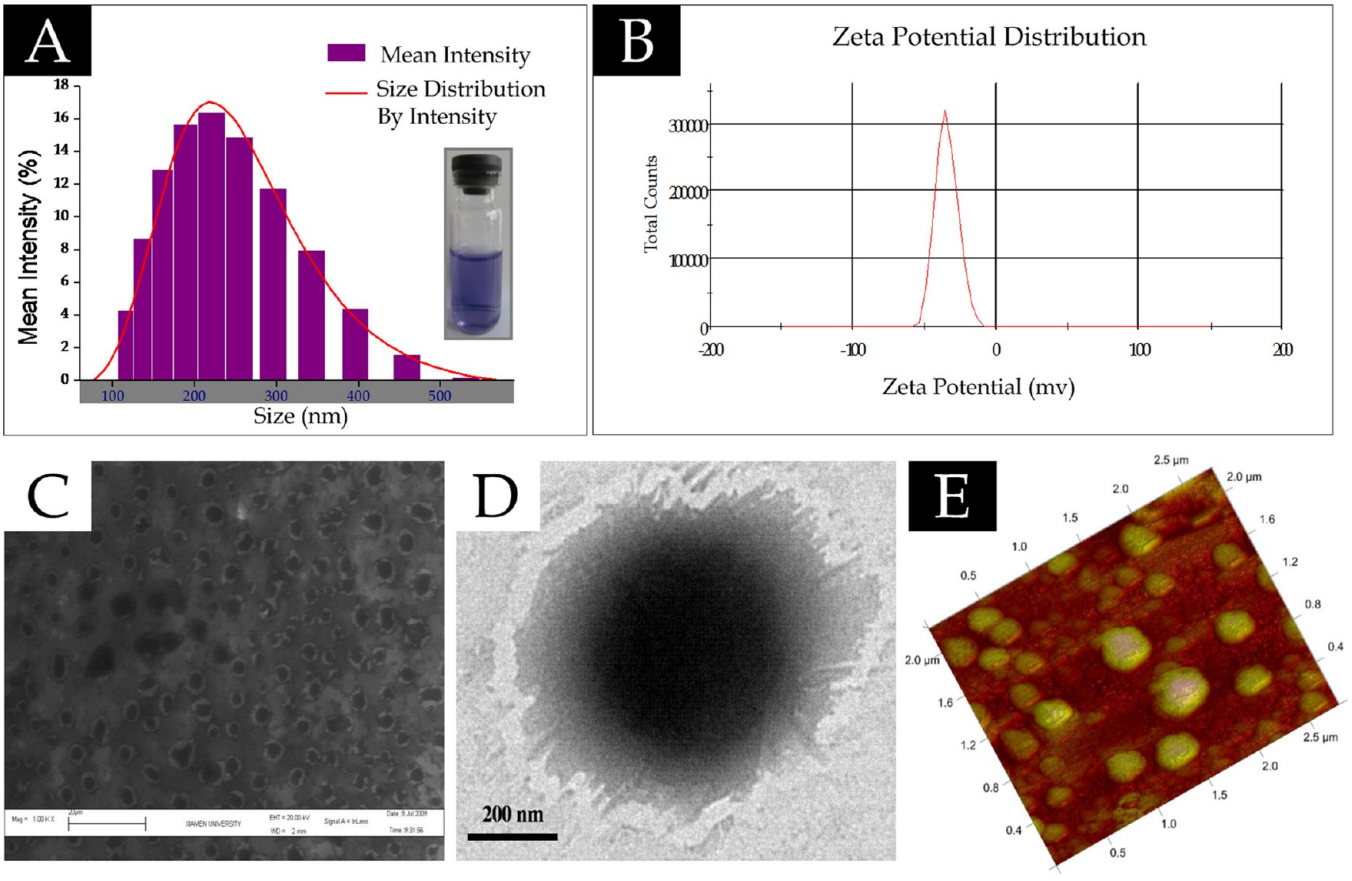

Figure 4. Physicochemical characterization of MMC-loaded phytosomes. (A) Particle size distribution of MMC-loaded phytosomes. Inset: photograph of as-prepared MMC-loaded phytosomes in a cuvette. (B) Zeta potential distribution of MMC-loaded phytosomes. (C) SEM image of MMC-loaded phytosomes. (D) TEM image of MMC-loaded phytosomes. (E) AFM image of MMC-loaded phytosomes.

The physicochemical state of incorporated drug in the subsequent phytosome nanoparticles is one important factor that affects the drug release behavior. Based on the spectral characteristics of DSC, XRD, and FTIR analysis of MMC, SPC, their physical mixture, and the MMC−SPC complex, it should be inferred synthetically that a certain interaction existed between MMC and the polar groups of SPC in the complex, while the two long nonpolar hydrocarbon chains of SPC were

dx.doi.org/10.1021/mp300489p | *Mol. Pharmaceutics* 2013, 10, 90−101

Table 1. The Average Particle Size, PDI, Zeta Potential, and Residual Drug-Loading Content of MMC-Loaded Phytosomes, before and after Lyophilization[a]

MMC-loaded phytosomes	av particle size (nm)	PDI	zeta potential (mV)	residual drug-loading content (%)
before lyophilization	210.87 ± 1.51	0.251 ± 0.019	−33.38 ± 0.33	100
after lyophilization	222.73 ± 1.44	0.261 ± 0.004	−33.40 ± 0.28	99.20 ± 0.57

[a]Values are mean ± SD, n = 3.

not participating in the complexation and could still turn freely to enwrap the polar parts to form a lipophilic appearance, thus these resulted in increase of lipophilicity and liposolubility of MMC in the complex essential for the subsequent preparation of the MMC-loaded phytosomes. Indeed, a series of spectra of the MMC−SPC complex reveal that MMC and SPC could form a molecule-based complex with no generation of new compounds, therefore the individual physicochemical properties of MMC and SPC will not change in vitro and in vivo.

3.2. Preparation and Characterization of MMC-Loaded Phytosomes. Mechanisms of the formation of the MMC-loaded phytosomes by a nanoprecipitation technique are schematically illustrated in Figure 3A. The first stage shows that the MMC−SPC complex dissolved in the organic phase and then diffused toward the continuous phase at a certain speed, leading to the drastic interface turbulence of the interface between the continuous phase and the organic phase, and subsequently the system turned into an O/W suspension; the second stage displayed that, due to some kind of interface instability arising from rapid diffusion of the organic phase across the interface, a dramatic decrease in the interfacial tension and a sharp increase in the interfacial area took place, resulting in a decrease perhaps of the droplet size of the complex, followed by spontaneous emulsification occurring without any external agitation or force; the third stage depicted further flow, diffusion, and surface processes, during which the organic phase further diffused into the continuous phase, while an excess amount of water further diffused into the nanodroplet, contributing to the formation of the phytosome nanoparticles; the fourth stage showed the continuous and gradual concentration of the already-formed nanoparticles due to the evaporation of the organic phase; the last stage depicted that, after the evaporation of the organic phase, the nanodroplets precipitated in the water environment, generating a system of phytosome nanoparticles loaded with the MMC−SPC complex. The representative structure illustration of the MMC-loaded phytosomes is depicted in Figure 3B.

The particle size has a major impact on the fate of a nanoparticle system as well as a size distribution. Additionally, monodisperse size distribution is essential for excellent physical stability. Zeta potential is a function of the surface charge of the suspension or dispersion, knowledge of which of the phytosomes can help to predict and control the fates of phytosome nanoparticles in vivo. Photographs of a size distribution and zeta potential distribution of the MMC-loaded phytosomes are depicted in Figures 4A and 4B, respectively. As is reported, the particle size (approximately 200 nm) and colloidal properties of lipid nanoparticles as drug delivery vehicles for the prolonged release of drugs played a rather important role in increasing the passive targeting efficiency of the reticuloendothelial system (RES).[37−39] So, an average particle size (210.87 ± 1.51 nm) of the MMC-loaded phytosomes with a narrow monodisperse size distribution (PDI 0.251 ± 0.019) is suitable for intravenous delivery. The zeta potential value (−33.38 ± 0.33 mV) observed for the MMC-loaded phytosomes was significantly lower than −30 mV (considered as the typical threshold for attraction and flocculation exceeding repulsion).[40] The high zeta potential of the produced phytosomes may be explained in that a great portion of SPC would be negatively charged in water environment with neutral pH value, making the phytosomes dynamically stable and suggesting the potential physical stability of drug in the phytosomes in the aqueous state. Overall, the small particle size, monodisperse size distribution, low PDI value, and high zeta potential indicated the excellent stability of the prepared phytosomes.

SEM, TEM, and AFM images (see Figures 4C, 4D, and 4E) of the MMC-loaded phytosomes exhibited mostly the shape of a liposome-like vesicle, relatively integrated structure, fairly uniform size, and well-distributed character dispersed in water environment. In our work, only SPC was used as the material for the delivery vehicle, and after complexing with MMC, the polar groups in the head of SPC molecules were effectively combined with MMC in the form of probably a hydrogen bond, obtaining a molecularly well-defined delivery vehicle.

3.3. Evaluation of Lyophilized MMC-Loaded Phytosomes. Lyophilization of the phytosome suspension could be performed to overcome either physical or chemical instability. The lyophilized MMC-loaded phytosomes could rapidly dissolve in distilled water and form a clear and homogeneous suspension with light bluish opalescence by gentle shaking for 10−15 s, similar to the freshly prepared MMC-loaded phytosomes. After reconstitution in distilled water, the average particle size became slightly larger, with PDI also higher compared to that of the MMC-loaded phytosomes before lyophilization, possibly ascribed to a partial aggregation between particles. It is worth pointing out that there was no obvious change in zeta potential and residual drug-loading content before and after lyophilization (see Table 1); the results substantially indicated no drug leakage from the MMC-loaded phytosomes after lyophilization.

Although the small particle size, the monodisperse and good particle size distribution, and the high zeta potential could preserve the stability of the phytosomes, it is well-known that if the phytosomes were in the state of suspension in a water environment for a long-term, the system would be destroyed, attributed to the physical instability (particle aggregation/fusion), the chemical instability (SPC hydrolysis from ester bonds, SPC oxidation, MMC leakage of nanoparticles) and/or the biological interference (bacterial growth).[41] The unexpected decreasing stability characteristics and labile activity in an aqueous suspension of phytosomes produced a real barrier against clinical application. Thus, the lyophilization technique was considered as a good technique and industrial process in the pharmaceutical field to reduce the physicochemical instability of phytosomes.

Dextran, serving as a cryprotectant in the lyophilization process, was used to improve the quality of the phytosomes. Overall, the fact suggested that the lyophilization developed in the present study was safe and guaranteed to ensure the

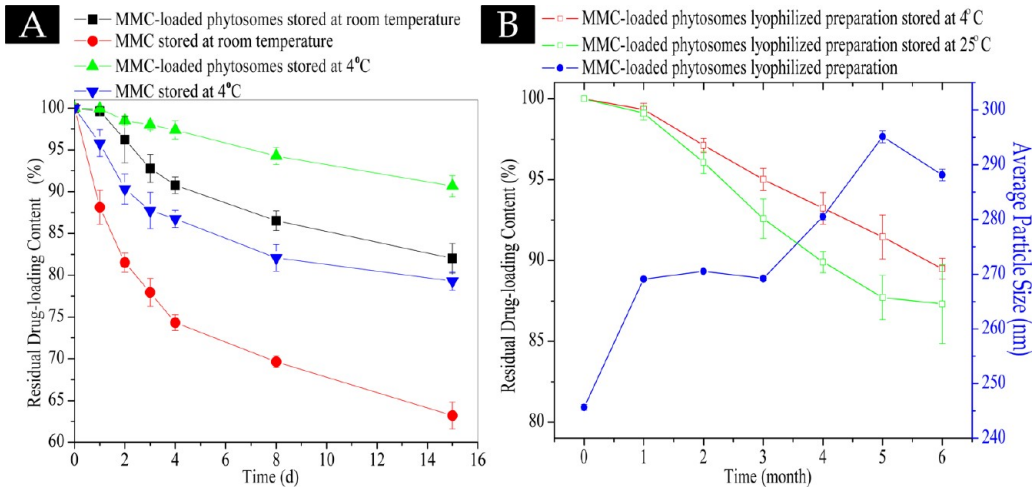

Figure 5. In vitro stability tests of MMC-loaded phytosomes. (A) The results of short-term stability tests of MMC and MMC-loaded phytosomes (the samples were stored for 15 days at 25 and 4 °C, respectively). (B) The results of long-term stability tests of lyophilized MMC-loaded phytosomes (the samples were stored for 6 months at 25 and 4 °C, respectively).

preservation of the physicochemical characteristics of the phytosomes without affecting the required quality essential for a good long-term stability of the formulation.

3.4. In Vitro Stability Tests. In vitro stability is one of the most critical factors of preparation in ensuring safety and efficacy of drug products. At the same time, it is a necessary step in the development processes and can provide evidence that the quality of drug product under the influence of various environmental factors changes with time, indicating the potentiality of industry production.

The results of a short-term stability test are illustrated in Figure 5A. There was a significant decrease in residual drug-loading content for free MMC solution stored at both 25 and 4 °C compared to the MMC-loaded phytosomes, suggesting that the MMC-loaded phytosomes in an aqueous environment could possess better stability than free MMC solution stored at two different temperatures for 15 days.

The long-term stability test was investigated in 6 months of storage at 4 and 25 °C in a dark place. The results of a long-term stability test are illustrated in Figure 5B. There was no significant change in 6 months about the average size and residual drug-loading content of the lyophilized MMC-loaded phytosomes. It is indicated that the MMC-loaded phytosomes formulated into lyophilized powder product containing excipients (2% of dextran-70, w/v) could markedly increase the stability of MMC. These results may be explained by the fact that drug-loaded phytosomes are regarded as a whole, in which drug exists in an amorphous state or a molecularly dispersed form and is fixed through the interaction with polar groups of SPC molecule. Therefore, in vitro stability tests verified that the affinity of MMC and SPC and the lipophilicity of the MMC−SPC complex can protect MMC against degradation.

3.5. In Vitro Release Profiles. An in vitro release profile reveals fundamental information on the structure and behavior of the formulation on a molecular level. Evaluation of in vitro release behavior was conducted to examine how rapidly MMC released from the MMC-loaded phytosomes. The output obtained by the dynamic dialysis method provided a correlation with in vivo drug release.

In vitro release behavior of MMC (commercial available MMC) and the MMC-loaded phytosomes is summarized in the accumulated release amount shown in Figure 6. The release profiles of MMC from the MMC-loaded phytosomes in either

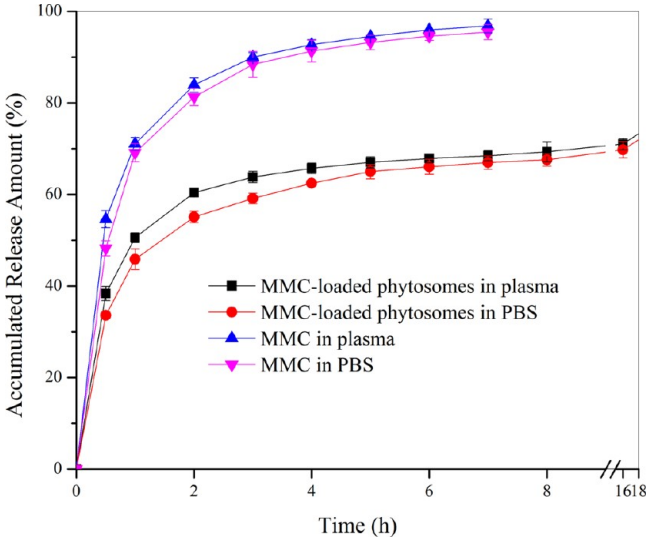

Figure 6. In vitro drug release profile of MMC from MMC-loaded phytosomes (the samples were suspended in either phosphate-buffered saline (PBS, 0.02 M, pH 7.4) or 25% (v/v) mouse plasma (PBS as the solvent) versus free MMC).

PBS or 25% plasma at 37 °C, showing a similar drug release behavior, can be divided into two phases: the first one considered as a burst release phase, and the second one considered as the sustained drug release phase. It is noteworthy that the release rate was slightly enhanced in plasma compared to PBS. As is reported, the high affinity of Rose Bengal with serum proteins resulted in the enhanced rate of Rose Bengal release from NPs,[42] so the affinity of MMC with plasma protein might promote the release of drug. In sharp contrast to MMC, a more sustained release status and depot effect and a longer time to reach release equilibruim were observed for the MMC-loaded phytosomes. The accumulative amount of MMC released from the MMC-loaded phytosomes was around 50% (either 45.87% in PBS or 50.57% in 25% plasma) in the first 1 h, and approximately 70% (either 67.57% in PBS or 69.34% in

dx.doi.org/10.1021/mp300489p | Mol. Pharmaceutics 2013, 10, 90−101

25% plasma) of the drug was released in 8 h. In comparison, the drug release from MMC solution was rather rapid conspicuously, with an accumulated release amount of almost 90% within 3 h, however, the amount of MMC release could not reach the 100% value, attributed to the inevitable and gradual disintegration in MMC aqueous solution.

The initial burst release behavior should be commonly ascribed to the presence of a certain amount of MMC−SPC complex absorbed on the surface of phytosomes; this phenomenon also suggested that the MMC−SPC complex trapped on the surface of phytosomes had suffered dissociation and MMC could be easily released in a free form. The later prolonged release behavior at a relatively low rate was greatly attributed to the location of the stable MMC−SPC complex effectively and homogeneously associated within the core spaces of phytosomes, and we suspected that the drug sustained transport out of phytosomes was a combination effect of the two stages, which was driven mainly by a diffusion-controlled mechanism; one was that MMC should be dissociated from the complex first and then free MMC within the core spaces diffused through a skeleton of phytosomes. These results indicated that the drug would be stable and release slowly in the blood circulation in vivo by an increase in the lipophilicity of drug attributed to the formation of the MMC−SPC complex and the subsequent incorporation of the complex into the MMC-loaded phytosomes; thus the MMC-loaded phytosomes would be expected to be an effective drug delivery system.

3.5. In Vitro Cytotoxicity Assays. Nanocytotoxicity is evaluated by the cell-killing performance of nanosystem. The cytotoxic activities of MMC and the MMC-loaded phytosomes were evaluated at different concentrations of MMC using the H_{22} cell line by a standard MTT assay.

As shown in Figure 7, the survival rate of H_{22} cells was totally suppressed in a drug dose-dependent manner by both the

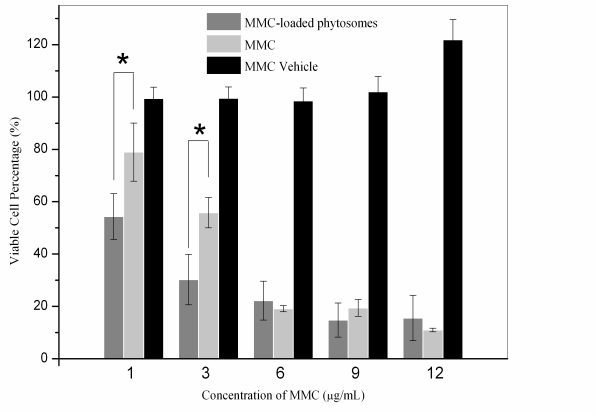

Figure 7. In vitro cytotoxicity assays for the growth inhibition effect of MMC, MMC-loaded phytosomes, and MMC vehicles in H_{22} cell after 24 h.

MMC-loaded phytosomes and MMC after 24 h of incubation. Interestingly, the low concentration (1 and 3 μg/mL) groups of the MMC-loaded phytosomes exhibited observably lower visible cell percentages than those of MMC solution group ($P < 0.05$), indicating that the MMC-loaded phytosomes (1 and 3 μg/mL) presented effectively higher cell-killing effciency compared with MMC solution. However, it should be stated that no obvious cell toxicity was found for the MMC vehicle, suggesting that the MMC vehicle is practically nontoxic, and therefore this safe material is worthy of being considered as an ideal nanocarrier for drug delivery and cancer therapy.

As is reported, the drug-loaded nanoparticle might be internalized by endocytosis thanks to their mesoscopic size, which virtually enhances the uptake of drug. At the same time, owing to the affinity of SPC to cells, lipid nanoparticles might maximize the permeability of drugs.[38,43−45] So, it may be assumed that the lipophilicity of MMC-loaded phytosomes facilitated the delivery of lipid nanoparticles to the interior of the cells across the phospholipid bilayer of cellular membranes, and then the phytosomes entering into cells could play the role of a drug storehouse, slowly generating high drug concentration and thus effectively enhancing cytotoxicity. On the contrary, the high concentration (6, 9, and 12 μg/mL) groups of the MMC-loaded phytosomes depicted a similar level of inhibition effect as MMC solution; this different phenomenon could be explained by cell penetration rate of drug depending on drug lipophilicity and drug concentration differences between the internal and external environment of the cell membrane. It should be emphasized that, in the case of a relatively low concentration of MMC, the lipophilicity of drug played a rather important role in the cell penetration rate of drug, however, in the case of a high concentration of MMC, the drug concentration differences played a main role. In vitro cytotoxicity study probably indicated that the MMC-loaded phytosomes at a certain range of the drug concentration may favorably suppress the activity of the H_{22} cells, thus it is expected that after intravenous injection, with the help of high affinity to cell surface, the phytosomes as a whole would easily enter into the interior of cancer cells to exert pharmacological effects. Nevertheless, these results need to be confirmed by other specific experiments.

3.6. In Vivo Antitumor Effects. In vivo antitumor effect of the MMC-loaded phytosomes was assessed using H_{22} solid tumor-bearing mice as the model animals. The body weight of mice in different groups all increased, but there were no significant differences between any two groups ($P > 0.05$) (see Table 2).

The first administration of 0.9% sodium chloride injection and MMC injection produced markedly faster tumor growth compared to that of the MMC-loaded phytosomes. After the second administration, the negative control group displayed active feeding/screaming, and the positive control group and high concentration experiment group showed some clinical symptoms, such as listlessness, reduced feeding, slight diarrhea, sleepiness, and hunched posture, believed to be the result of the side effects of MMC. The low and medium concentration experiment groups showed no phenomena mentioned above. It can be apparently seen that the side effects of the positive control group are conspicuous. Since the tumor weight in different groups was all less than 6% of the initial body weight, the increase in body weight should not be ascribed solely to the growth of tumor,[37] implying that the MMC-loaded phytosomes were well tolerated at all treatment dose levels.

As shown in Table 2, the tumor growth was inhibited dose-dependently by the MMC-loaded phytosomes. All experiment groups reflected significantly obvious suppression of tumor growth ($P < 0.005$) compared to the positive control group treated with 2 mg/kg of free drug injection. This dosing schedule was adequate for treatment using the MMC-loaded phytosomes. It was also noted that the inhibition rate of 2 mg/

dx.doi.org/10.1021/mp300489p | Mol. Pharmaceutics 2013, 10, 90−101

Table 2. In Vivo Antitumor Effects in H_{22} Bearing Kunming Male Mice[a]

item	negative	positive	low	medium	high
N	10	10	10	10	10
death	0	0	0	0	0
initial (g)	19.04 ± 0.75	19.23 ± 1.22	19.35 ± 1.30	19.55 ± 0.61	20.88 ± 0.82
final (g)	26.88 ± 1.19	24.75 ± 2.04	25.86 ± 1.87	24.16 ± 1.69	24.93 ± 0.97
TW (g)	0.33 ± 0.08	0.31 ± 0.14	0.18 ± 0.06[b]	0.13 ± 0.04*	0.12 ± 0.03*
TIR (%)	N/A	9.82 ± 23.33	45.09 ± 10.00*	61.32 ± 8.94*	64.02 ± 1.76*

[a]Negative: Negative control group treated with 0.9% sodium chloride injection. Positive: Positive control group treated with MMC injection at 2 mg/kg. Low: Low concentration group (1 mg/kg). Medium: Medium concentration group (2 mg/kg). High: High concentration group (3 mg/kg). *N*: Number of mice. Death: Number of mouse deaths during 12 days of experiment. Initial: Initial average of body weight. Final: Final average of body weight. TW: average weight of tumor. TIR: tumor inhibition rate. [b]*$P < 0.005$ compared with positive control group.

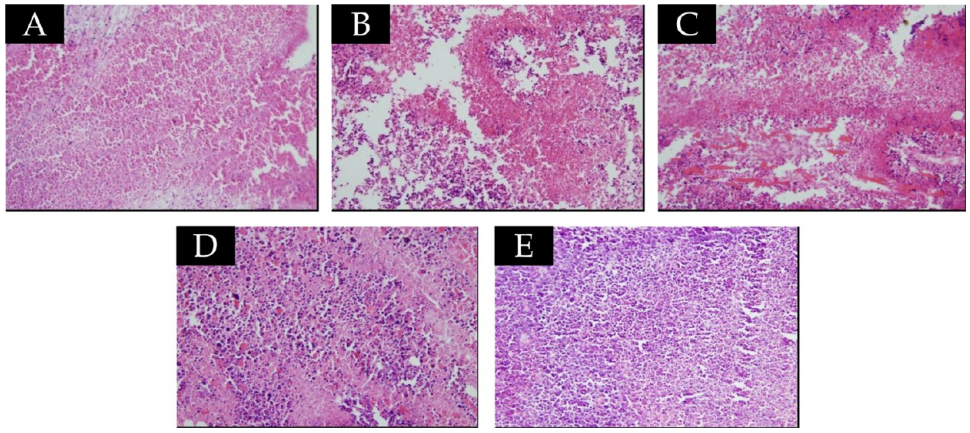

Figure 8. Representative photomicrographs of histopathological sections of the tumor tissues from tumor-bearing mice (HE stained, magnification 200×). (A) Treatment with high dose of MMC-loaded phytosomes group (3 mg/kg). (B) Treatment with middle dose of MMC-loaded phytosomes group (2 mg/kg). (C) Treatment with low dose of MMC-loaded phytosomes group (1 mg/kg). (D) Treatment with MMC injection group (2 mg/kg). (E) Treatment with negative control group.

kg of the MMC-loaded phytosomes was 61.32 ± 8.94%, which was approximately 6-fold of free drug injection at the equivalent concentration.

The overall in vivo antitumor effects indicated that the MMC-loaded phytosomes markedly possessed more powerful antitumor activity compared to MMC injection. We concluded that the following factors may be involved: First, nanoparticles can help the incorporated drug enter the interior of cells and circumvent the MDR mechanism.[44,46] Consequently, the MMC-loaded phytosomes can be endocytosed more easily and utilized more effectively by cancer cells after intravenous administration. Second, the biological half-life of MMC is very short and the effective time of drug in systemic circulation is very short, and thus the drug concentration is very low when drug reached to the local area of the tumor, whereas the sustained-release characteristic of the MMC-loaded phytosomes may result in a prolonged exposure of the tumor cells to the attack of the antitumor drug. Last, the lipophilicity of drug-loaded phytosomes powerfully helps the drug molecule transport across lipid-rich cell membranes and enter the internal environment of the cells, leading to high drug concentration and exhibiting great activity against the cancer cell, thus resulting in effective antitumor efficiency at a specific range of the administration dose. So, the present study suggested that the MMC-loaded phytosomes would be useful in significantly enhancing the antitumor effect of MMC compared to MMC injection in vivo administration and providing a valuable means for intravenous injection clinical treatment.

3.7. Histopathologic Analysis. Histopathologic analysis of tumor tissues from H_{22} solid tumor-bearing mice gave a visual assessment of cellular architecture. The different antitumor efficiency caused by MMC could be clearly distinguished by the degree of putrescence and degeneration of tumor cells in each group. Through biomicroscopy (L2000A) with conventional HE staining, representative microscopic images of paraffin sections of tumor tissues with 5 groups are illustrated in Figure 8. The mice treated with the negative control group (Figure 8E) showed visible sheets of dense tumor cells with vigorous tumor cell division−proliferation and intact vessels, indicating little cell death after treatment with the negative control group. Treatment of animals with MMC injection group (2 mg/kg) resulted in unremarkable antitumor efficiency as can be observed from remaining activities of tumor cell division−proliferation and slight area of cell death (Figure 8D). Treatment of animals with the MMC-loaded phytosomes group (1 mg/kg) resulted in a certain extent of antitumor efficiency, as can be observed by visible degeneration of tumor cells and midrange cell death (Figure 8C). As compared to treatment of animals with the other groups, the vessels were injured and significantly severe cell death was observed on treatment of animals with the MMC-loaded phytosomes groups (2 and 3 mg/kg) (Figures 8B and 8A). Pathological examinations illustrated that increasing the concentration of the MMC-loaded phytosomes resulted in a proportionate increase of cell death in tumor tissue, indicating that the MMC-loaded phytosomes were cytostatic and lethal to tumor cells in a dose-dependent manner. So, a dose-dependent different

dx.doi.org/10.1021/mp300489p | *Mol. Pharmaceutics* 2013, 10, 90−101

action indicates that the dosage of drug must be critically controlled for applying hepatocellular carcinoma therapy. Therefore, these results suggested that the MMC-loaded phytosomes could play an effective role of antitumor effect.

4. CONCLUSION

In this present study, a simple but successful method was developed to obtain a novel formulation of the MMC-loaded phytosomes with improved formulation characteristics including smaller size, lower size distribution, higher zeta potential, and better stability. The MMC-loaded phytosomes exhibited remarkably high cytotoxicity as well as superior inhibition effect compared to MMC. Nevertheless, more details about in vivo antitumor investigation, including in vivo biodistribution and pharmacokinetics of the MMC phytosomes, are indispensable to obtain a better understanding of the therapeutic effect of the MMC-loaded phytosomes, and relevant studies are in process.

AUTHOR INFORMATION

Corresponding Author

*Department of Biomaterials, Research Center of Biomedical Engineering, Xiamen University, Xiamen 361005, China, and Institute of Biomedical Engineering, Chinese Academy of Medical Science, Peking Union Medical College, The Key Laboratory of Biomaterial of Tianjin, Tianjin 00192, China. Tel: +086 592 2184476. Fax: +086 2287890868. E-mail: Zhangqiq@xmu.edu.cn (Q.Z.), Houzhenqing@xmu.edu.cn (Z.H.).

Author Contributions

‡These authors contributed equally to this work.

Notes

The authors declare no competing financial interest.

ACKNOWLEDGMENTS

This work was funded by the Major Research Plan of the National Natural Science Foundation of China (Grant No.90923042), the National Natural Science Foundation of China (Grant No.81000660, 31271071), and Xiamen Science and Technology Project (3500Z20123001).

ABBREVIATIONS USED

MMC, mitomycin C; SPC, soybean phosphatidylcholine; DSC, differential scanning calorimetry; FTIR, Fourier transform infrared spectroscopy; XRD, X-ray diffraction; DLS, dynamic light scattering; SLS, static light scattering; SEM, scanning electron microscopy; TEM, transmission electron microscopy; AFM, atomic force microscope; HPLC, high-performance liquid chromatography

REFERENCES

(1) Schwartz, H. S.; Sodergren, J. E.; Philips, F. S. Mitomycin C: Chemical and Biological Studies on Alkylation. *Science* **1963**, *142* (3596), 1181−1183.

(2) Iyer, V. N.; Szybalski, W. Mitomycins and Porfiromycin: Chemical Mechanism of Activation and Cross-Linking of DNA. *Science* **1964**, *145* (3627), 55−58.

(3) Bradner, W. T. Mitomycin C: a clinical update. *Cancer Treat. Rev.* **2001**, *27* (1), 35−50.

(4) Boamah, E. K.; White, D. E.; Talbott, K. E.; Arva, N. C.; Berman, D.; Tomasz, M.; et al. Mitomycin-DNA adducts induce p53-dependent and p53-independent cell death pathways. *ACS Chem. Biol.* **2007**, *2* (6), 399−407.

(5) den Hartigh, J.; McVie, J. G.; van Oort, W. J.; Pinedo, H. M. Pharmacokinetics of mitomycin C in humans. *Cancer Res.* **1983**, *43* (10), 5017−5021.

(6) Tomasz, M.; Lipman, R.; Chowdary, D.; Pawlak, J.; Verdine, G. L.; Nakanishi, K. Isolation and structure of a covalent cross-link adduct between mitomycin C and DNA. *Science* **1987**, *235* (4793), 1204−1208.

(7) Hall, T. C. Chemotherapy of cancer. *N. Engl. J. Med.* **1962**, *266*, 289−296.

(8) Hanna, W. T.; Krauss, S.; Regester, R. F.; Murphy, W. M. Renal disease after mitomycin C therapy. *Cancer* **1981**, *48* (12), 2583−2588.

(9) Rumpf, K. W.; Rieger, J.; Lankisch, P. G.; von Heyden, H. W.; Nagel, G. A.; Scheler, F. Mitomycin-induced haemolysis and renal failure. *Lancet* **1980**, *2* (8202), 1037−1038.

(10) Zein, T. A.; Friedberg, N.; Kim, H. Bone marrow suppression after intravesical mitomycin C treatment. *J. Urol.* **1986**, *136* (2), 459−460.

(11) Minelli, C.; Lowe, S. B.; Stevens, M. M. Engineering nanocomposite materials for cancer therapy. *Small* **2010**, *6* (21), 2336−2357.

(12) Rozhkova, E. A. Nanoscale materials for tackling brain cancer: recent progress and outlook. *Adv. Mater.* **2011**, *23* (24), H136−150.

(13) Constantinides, P. P.; Chaubal, M. V.; Shorr, R. Advances in lipid nanodispersions for parenteral drug delivery and targeting. *Adv. Drug Delivery Rev.* **2008**, *60* (6), 757−767.

(14) Kidd, P. M. Bioavailability and activity of phytosome complexes from botanical polyphenols: the silymarin, curcumin, green tea, and grape seed extracts. *Altern. Med. Rev.* **2009**, *14* (3), 226−246.

(15) Bildstein, L.; Dubernet, C.; Couvreur, P. Prodrug-based intracellular delivery of anticancer agents. *Adv. Drug Delivery Rev.* **2011**, *63* (1−2), 3−23.

(16) Chan, J. M.; Zhang, L.; Yuet, K. P.; Liao, G.; Rhee, J. W.; Langer, R.; et al. PLGA-lecithin-PEG core-shell nanoparticles for controlled drug delivery. *Biomaterials* **2009**, *30* (8), 1627−1634.

(17) Fricker, G.; Kromp, T.; Wendel, A.; Blume, A.; Zirkel, J.; Rebmann, H.; et al. Phospholipids and lipid-based formulations in oral drug delivery. *Pharm. Res.* **2010**, *27* (8), 1469−1486.

(18) Bombardelli, E. Phytosome: new cosmetic delivery system. *Boll. Chim. Farm.* **1991**, *130* (11), 431−438.

(19) Peer, D.; Karp, J. M.; Hong, S.; Farokhzad, O. C.; Margalit, R.; Langer, R. Nanocarriers as an emerging platform for cancer therapy. *Nat. Nanotechnol.* **2007**, *2* (12), 751−760.

(20) Soussan, E.; Cassel, S.; Blanzat, M.; Rico-Lattes, I. Drug delivery by soft matter: matrix and vesicular carriers. *Angew. Chem., Int. Ed.* **2009**, *48* (2), 274−288.

(21) Dahan, A.; Duvdevani, R.; Shapiro, I.; Elmann, A.; Finkelstein, E.; Hoffman, A. The oral absorption of phospholipid prodrugs: in vivo and in vitro mechanistic investigation of trafficking of a lecithin-valproic acid conjugate following oral administration. *J. Controlled Release* **2008**, *126* (1), 1−9.

(22) Federico, A.; Trappoliere, M.; Tuccillo, C.; de Sio, I.; Di Leva, A.; Del Vecchio Blanco, C.; et al. A new silybin-vitamin E-phospholipid complex improves insulin resistance and liver damage in patients with non-alcoholic fatty liver disease: preliminary observations. *Gut* **2006**, *55* (6), 901−902.

(23) Lu, Y.; Zhang, Y.; Yang, Z.; Tang, X. Formulation of an intravenous emulsion loaded with a clarithromycin-phospholipid complex and its pharmacokinetics in rats. *Int. J. Pharm.* **2009**, *366* (1−2), 160−169.

(24) Maiti, K.; Mukherjee, K.; Gantait, A.; Saha, B. P.; Mukherjee, P. K. Curcumin-phospholipid complex: Preparation, therapeutic evaluation and pharmacokinetic study in rats. *Int. J. Pharm.* **2007**, *330* (1−2), 155−163.

(25) Peng, Q.; Zhang, Z. R.; Sun, X.; Zuo, J.; Zhao, D.; Gong, T. Mechanisms of phospholipid complex loaded nanoparticles enhancing the oral bioavailability. *Mol. Pharmaceutics* **2010**, *7* (2), 565−575.

(26) Singh, D.; Rawat, M. S.; Semalty, A.; Semalty, M. Rutin-phospholipid complex: an innovative technique in novel drug delivery system-NDDS. *Curr. Drug Delivery* **2012**, *9* (3), 305−314.

(27) Wei, W.; Shi, S. J.; Liu, J.; Sun, X.; Ren, K.; Zhao, D.; et al. Lipid nanoparticles loaded with 10-hydroxycamptothecin-phospholipid complex developed for the treatment of hepatoma in clinical application. *J. Drug Targeting* **2010**, *18* (7), 557−566.
(28) Xu, K.; Liu, B.; Ma, Y.; Du, J.; Li, G.; Gao, H.; et al. Physicochemical properties and antioxidant activities of luteolin-phospholipid complex. *Molecules* **2009**, *14* (9), 3486−3493.
(29) Yanyu, X.; Yunmei, S.; Zhipeng, C.; Qineng, P. The preparation of silybin-phospholipid complex and the study on its pharmacokinetics in rats. *Int. J. Pharm.* **2006**, *307* (1), 77−82.
(30) Yue, P. F.; Yuan, H. L.; Li, X. Y.; Yang, M.; Zhu, W. F. Process optimization, characterization and evaluation in vivo of oxymatrine-phospholipid complex. *Int. J. Pharm.* **2010**, *387* (1−2), 139−146.
(31) Zhang, Z.; Huang, Y.; Gao, F.; Bu, H.; Gu, W.; Li, Y. Daidzein-phospholipid complex loaded lipid nanocarriers improved oral absorption: in vitro characteristics and in vivo behavior in rats. *Nanoscale* **2011**, *3* (4), 1780−1787.
(32) Cui, F.; Shi, K.; Zhang, L.; Tao, A.; Kawashima, Y. Biodegradable nanoparticles loaded with insulin-phospholipid complex for oral delivery: preparation, in vitro characterization and in vivo evaluation. *J. Controlled Release* **2006**, *114* (2), 242−250.
(33) Peng, Q.; Zhang, Z. R.; Gong, T.; Chen, G. Q.; Sun, X. A rapid-acting, long-acting insulin formulation based on a phospholipid complex loaded PHBHHx nanoparticles. *Biomaterials* **2012**, *33* (5), 1583−1588.
(34) Hou, Z.; Wei, H.; Wang, Q.; Sun, Q.; Zhou, C.; Zhan, C.; et al. New Method to Prepare Mitomycin C Loaded PLA-Nanoparticles with High Drug Entrapment Efficiency. *Nanoscale Res. Lett.* **2009**, *4* (7), 732−737.
(35) Lasonder, E.; Weringa, W. D. An NMR and DSC study of the interaction of phospholipids vesicles with some anti−inflammatory agents. *J. Colloid Interface Sci.* **1990**, *139* (2), 469−478.
(36) Lucio, M.; Bringezu, F.; Reis, S.; Lima, J. L.; Brezesinski, G. Binding of nonsteroidal anti-inflammatory drugs to DPPC: structure and thermodynamic aspects. *Langmuir* **2008**, *24* (8), 4132−4139.
(37) Zhang, L.; Yang, M.; Wang, Q.; Li, Y.; Guo, R.; Jiang, X.; et al. 10-Hydroxycamptothecin loaded nanoparticles: preparation and antitumor activity in mice. *J. Controlled Release* **2007**, *119* (2), 153−162.
(38) Soma, C. E.; Dubernet, C.; Barratt, G.; Benita, S.; Couvreur, P. Investigation of the role of macrophages on the cytotoxicity of doxorubicin and doxorubicin-loaded nanoparticles on M5076 cells in vitro. *J. Controlled Release* **2000**, *68* (2), 283−289.
(39) Xu, Z.; Chen, L.; Gu, W.; Gao, Y.; Lin, L.; Zhang, Z.; et al. The performance of docetaxel-loaded solid lipid nanoparticles targeted to hepatocellular carcinoma. *Biomaterials* **2009**, *30* (2), 226−232.
(40) Bonincontro, A.; Falivene, M.; Mesa, C. L.; Risuleo, G.; Pena, M. R. Dynamics of DNA adsorption on and release from SDS-DDAB cat-anionic vesicles: a multitechnique study. *Langmuir* **2008**, *24* (5), 1973−1978.
(41) Abdelwahed, W.; Degobert, G.; Stainmesse, S.; Fessi, H. Freeze-drying of nanoparticles: formulation, process and storage considerations. *Adv. Drug Delivery Rev.* **2006**, *58* (15), 1688−1713.
(42) Redhead, H. M.; Davis, S. S.; Illum, L. Drug delivery in poly(lactide-co-glycolide) nanoparticles surface modified with poloxamer 407 and poloxamine 908: in vitro characterisation and in vivo evaluation. *J. Controlled Release* **2001**, *70* (3), 353−363.
(43) Partlow, K. C.; Lanza, G. M.; Wickline, S. A. Exploiting lipid raft transport with membrane targeted nanoparticles: a strategy for cytosolic drug delivery. *Biomaterials* **2008**, *29* (23), 3367−3375.
(44) Savic, R.; Luo, L.; Eisenberg, A.; Maysinger, D. Micellar nanocontainers distribute to defined cytoplasmic organelles. *Science* **2003**, *300* (5619), 615−618.
(45) Xiong, X. B.; Huang, Y.; Lu, W. L.; Zhang, X.; Zhang, H.; Nagai, T.; et al. Enhanced intracellular delivery and improved antitumor efficacy of doxorubicin by sterically stabilized liposomes modified with a synthetic RGD mimetic. *J. Controlled Release* **2005**, *107* (2), 262−275.
(46) Brigger, I.; Dubernet, C.; Couvreur, P. Nanoparticles in cancer therapy and diagnosis. *Adv. Drug Delivery Rev.* **2002**, *54* (5), 631−651.